Wind and Structures, *Vol. 32, No. 1 (2021) 55-69*
DOI: https://doi.org/10.12989/was.2021.32.1.55

Wind resistance performance of a continuous welding stainless steel roof under static ultimate wind loading with testing and simulation methods

Dayang Wang[1], Zhendong Zhao[2], Tong Ou[3], Zhiyong Xin[4], Mingming Wang[1] and Yongshan Zhang*[1]

[1]*School of Civil Engineering, Guangzhou University, 510006, P.R. China*
[2]*State Key Laboratory of Nuclear Power Safety Monitoring Technology and Equipment, China Nuclear Power Engineering Co. Ltd., Shenzhen 518172, China*
[3]*Architectural Design and Research Institute of Guangdong Province, 510000, P.R. China*
[4]*Zhuhai Envete Engineering Testing Co., LTD, 519000, P.R. China*

(*Received August 11, 2020, Revised January 2, 2021, Accepted January 22, 2021*)

Abstract. Ultrapure ferritic stainless steel provides a new generation of long-span metal roof systems with continuous welding technology, which exhibits many unknown behaviors during wind excitation. This study focuses on the wind-resistant capacity of a new continuous welding stainless steel roof (CWSSR) system. Full-scale testing on the welding joints and the CWSSR system is performed under uniaxial tension and static ultimate wind uplift loadings, respectively. A finite element model is developed with mesh refinement optimization and is further validated with the testing results, which provides a reliable way of investigating the parameter effect on the wind-induced structural responses, namely, the width and thickness of the roof sheeting and welding height. Research results show that the CWSSR system has predominant wind-resistant performance and can bear an ultimate wind uplift loading of 10.4 kPa without observable failures. The welding joints achieve equivalent mechanical behaviors as those of base material is produced with the current of 65 A. Independent structural responses can be found for the roof sheeting of the CWSSR system, and the maximum displacement appears at the middle of the roof sheeting, while the maximum stress appears at the connection supports between the roof sheeting with a significant stress concentration effect. The responses of the CWSSR system are greatly influenced by the width and thickness of the roof sheeting but are less influenced by the welding height.

Keywords: metal roof system; continuous welding; wind resistance performance; full-scale testing; numerical simulation

1. Introduction

Metal roof systems with the characteristics of high-strength and lightweight materials have been widely accepted for large-span lower-level structures, such as airports, train stations, and industrial workshops. Nearly 65% of lower-level buildings in the United States have adopted this roof system according to statistical information from the Metal Building Manufacturers Association (Dabral and Ewing 2009, Ji and Huang 2018). Most researches focus on the surface wind pressure distribution (Stathopoulos and Wang 2001, Banks and Meroney 2001, Uematsu and Yamada 2002) and load calculation methods (Lovisa and Wang 2013, Luo and Liao 2017) of the roof structure, and there is very little research on the metal roof system. Thin-walled and large-span members are typical types of components of metal roof systems, which, are vulnerable to premature connection failures and cause heavy losses when subjected to strong wind events such as storms and cyclones, according to postevent damage investigations (Holmes 2015, Baskaran and Molleti 2007, NIST 2006). Moreover, connection failures will inevitably cause leakage problems for roof sheeting during strong wind excitation, which will be disastrous to the contents of a building and result in business interruption. Obviously, researching the wind-resistance performance of large-span metal roof systems is an interesting and valuable topic to ensure disaster safety and avoid extensive loss.

Pull-out failure and pull-through failure are two main localized roof connection failures (Sivapathasundaram and Mahendran 2018). The former refers to screw fasteners of roof connections pulling out from roof battens or purlins, and the latter refers to screw fasteners pulling through the metal roof sheeting. Fruitful test investigations and calculation theories on pull-through or pull-out failures have been conducted and proposed by researchers (Mahendran 1997, Xu and Reardon 1993, Mahaarachchi 2009, Mahendran 1995), aiming to improve the wind-resistance performance of these connections. Adopting cyclone washers with screw fasteners is suggested by Xu and Reardon (1993) to reduce local plastic deformations and increase initial failure loads of roof sheeting, which, is found to be insufficient for pull-out failure in recent wind failure investigations (Boughton and Falck 2007). Tests on 592 small-scale specimens were carried out to study traditional screw fasteners and their performance when pulling out from steel battens, purlins and girts by Mahendran and Tang (Mahendran and Tang 1998); it is recommended that a reduced capacity factor of 0.4 be considered to achieve a more suitable design formula according to experimental investigations. A total of 187

*Corresponding author, Professor
E-mail: cezhangyongshan@gzhu.edu.cn

ISSN: 1226-6116 (Print), 1598-6225 (Online)

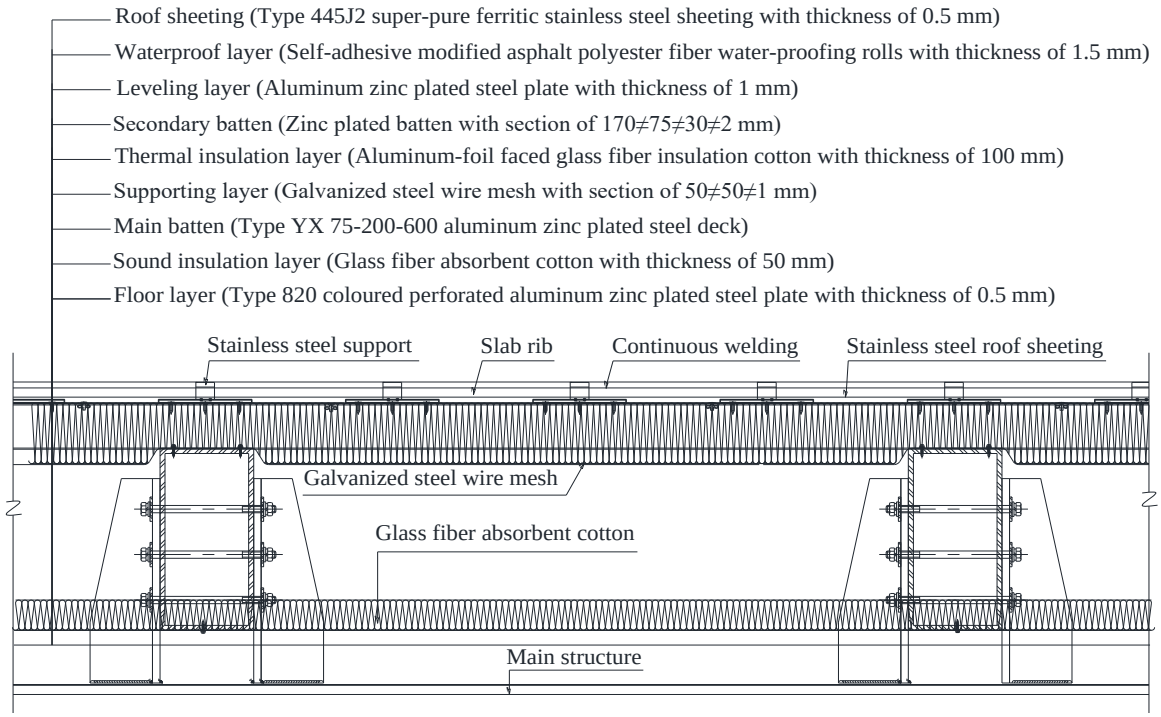

(a) Geological section diagram

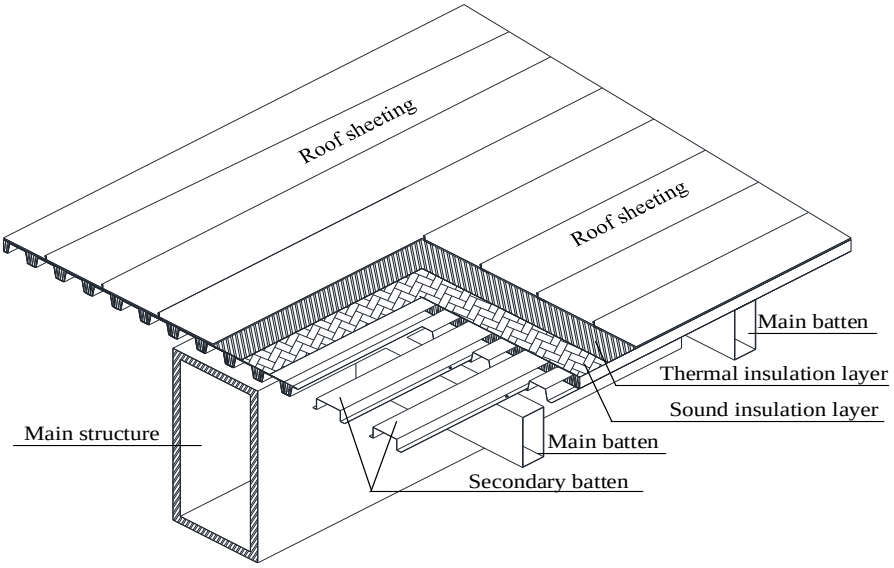

(b) Three dimensional diagram

Fig. 1 Structure of the CWSSR system in the Zhaoqing New District Sports Center

small-scale pull-out tests with new screw fasteners, which are currently used more frequently, are further performed by Sivapathasundaram and Mahendran (2018) to study pull-out failures, and new design equations of these connections are developed based on the corresponding tests, together with the previous 592 test results. In addition, a wind-induced disaster damage assessment has also attracted wide attention, which highlights the importance of uncertainty analysis (Ji and Huang 2018) and develops many valuable assessment methods, such as the database-assisted vulnerability damage estimation method (Zhao and Gu 2011, Huang and He 2015), probabilistic risk assessment method (Li and Ellingwood 2006), and roof vulnerability model excited by tropical cyclones (Konthesingha and Stewart 2005).

Although many improvements have been made, premature failures of the screw and seam-clip connections for traditional roof systems, such as widely used standing seam metal roof systems, have occurred frequently in strong winds. This is because this open roof system adopts weak seam-clip connections between the roof sheeting and its supports, in which the force transfer mechanism is complicated and unstable; disengaging failure of the seam-clip connection is usually caused by wind excitation (Friedrich and Luible 2016, Damatty and Rahman 2003). To ensure an integral and substantial roof system, a new

continuous welding stainless steel roof (CWSSR) system is developed, which transforms the traditional seam-clip connection into a welded connection between two adjacent roof sheetings, and between roof sheeting and its supports. Although few applications have been realized in recent years for the new CWSSR system, such as the Rotterdam Central Railway Station of the Netherlands, Tokyo Haneda International Airport terminal of Japan and Zhaoqing New District Sports Center of China, they have not yet been well addressed in wind resistance studies, and very limited literature can be found on this topic. To develop a comprehensive understanding of the new CWSSR system in wind excitations, one needs to integrate the wind-induced performance investigation on the joint mechanical behavior, cooperative wind-resistance capacity, and parameter effect.

With these considerations, this study is organized as follows. First, the new CWSSR system and the corresponding computational model are introduced. Second, the mechanical properties of 15 welding joints of the roof sheeting are tested to examine the connection behaviors and provide support data to the computational model. Third, a full-scale testing investigation of the CWSSR system under static ultimate wind uplift loading is performed to explore the wind resistance performance and to further validate the numerical analyses. Fourth, investigations on the parameter effects, namely the thickness and width of the roof sheeting and welding height, are discussed in detail to determine the influence tendency of such parameters for references of the actual engineering design and also further research. Finally, concluding remarks are given.

2. Overview of the CWSSR system

The CWSSR system studied in this investigation is from a real structure, named the Zhaoqing New District Sports Center, which was built in 2018 and was the first large-scale application of the CWSSR system in China. The CWSSR system is a complex structural composition, including main bearing structural members and nonbearing functional members, as shown in Fig. 1. The bearing structural members are made up of the roof sheeting, secondary batten, and main batten. All others, such as waterproof, leveling, and thermal insulation layers are nonbearing functional members. Type 445J2 ultrapure ferritic stainless steel is adopted as the material of the roof sheeting, which has a width of 400 mm, a thickness of 0.5 mm, the yield strength of 329 MPa, an elasticity modulus of 200 GPa, a Poisson's ratio of 0.3, and a density of 7.75 g/cm3. The length of the roof sheeting is determined by the specific structural span and varies from different positions. The stainless steel support is designed between the roof sheeting and secondary batten along the longitudinal direction with a spacing of 300 mm. Adjacent stainless steel roof sheeting is welded continuously along the longitudinal direction with a movable electric-resistance welder. The roof sheeting is also welded to the upper part of the stainless steel support, while the lower part of the support is connected to the secondary batten with screw fasteners. The welding height is 17 mm from the bottom of the roof sheeting.

3. Finite element model

As introduced in the last section, the CWSSR system is a complex structural composition. It will be very difficult to consider all the bearing and functional members in numerical simulation. As an alternative, the bearing structural members, namely, the roof sheeting, welding joints, and supports, are taken into account, which is reasonable as those nonbearing functional members do not contribute to the bearing capacity of the CWSSR system during wind excitation (Damatty and Rahman 2003, Wang and Wu 2019). Wind loading is undertaken firstly by the roof sheeting and then transmitted to the stainless steel supports. The supports finally transmit the loading to the secondary battens by means of screw fasteners. Obviously, the screw fasteners are the key force-transfer members, which are validated as intact without any damage or local failure due to static ultimate wind uplift testing (Ou and Wang 2020) and will be confirmed in the following section. In other words, the typical pull-out failure that occurs frequently in traditional roof systems under strong winds is avoided by the CWSSR system. Thus, the screw connections between the supports and the secondary batten are simulated as fixed constraints.

The investigated geometry of the CWSSR system is rectangular with a plan dimension of 6300 mm × 3820 mm, which meets the testing size requirements of the standards of CSA-A123.21-14 (2015) and ASTM E1592-05 (2017). Figs. 2 and 3 show the plan and the corresponding cross-section of the investigated roof sheeting, respectively. Constraints on the four sides of the CWSSR system are defined as fixed connections, which is consistent with the actual situation. All welding connections between adjacent roof sheeting members and between the roof sheeting and supports are also defined to be fixed connections. The reason for such numerical treatment will be validated by the following experimental investigation on the mechanical behaviors of the welding joints, which illustrates that the continuous welding joints generated by a movable electric-resistance welder can achieve the equivalent mechanical performance of the base material. Thus, the key point of the numerical model of the CWSSR system is to simulate the roll-up position between adjacent roof sheeting members and the flexible position in the middle of the roof sheeting, as shown in Fig. 2(b). This is because the two positions are geometrically discontinuous and prone to stress concentration. Analysis of the mesh refinement (MR) on the roll-up position and flexible position, defined as MR-R and MR-F, respectively, is herein adopted to achieve reliable results considering factors of computational efficiency and accuracy (Wang and Zhuang 2018, Wang and Tse 2015).

The general-purpose computer code ANSYS (Ansys release 2011) is employed to perform the finite element analyses of the CWSSR system under wind loading. Both roof sheeting and supports of the CWSSR system are simulated by a four-node quadrilateral shell element, which has bending and membrane properties with six DOFs, namely, three-direction translational displacement and three-direction rotational displacement. The stiffness and mass matrices and all related components are based on 2 ×

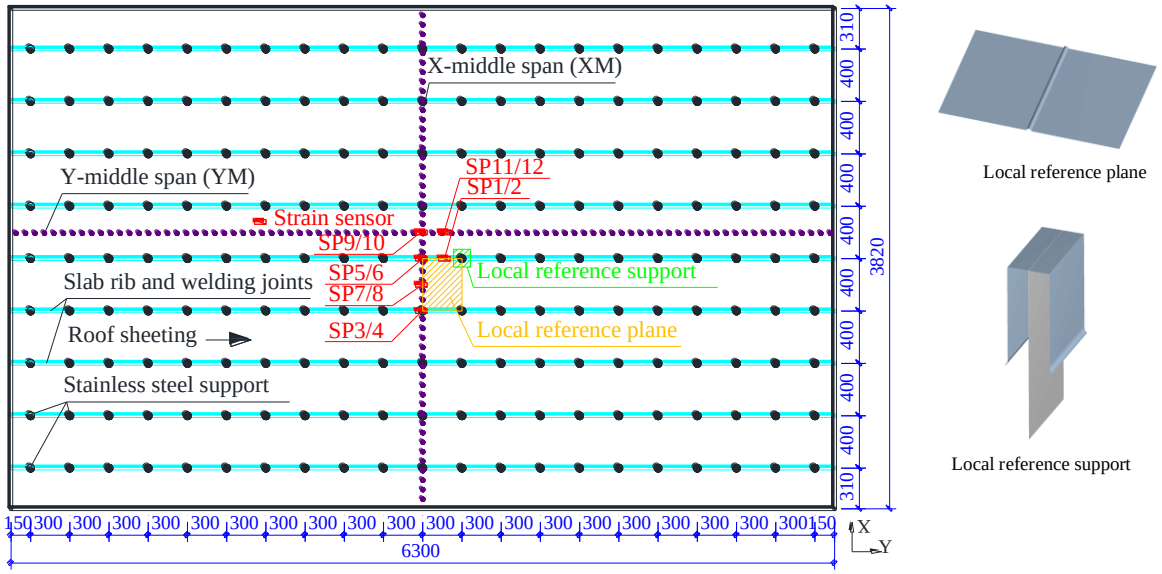

(a) Plane layout local finite element model

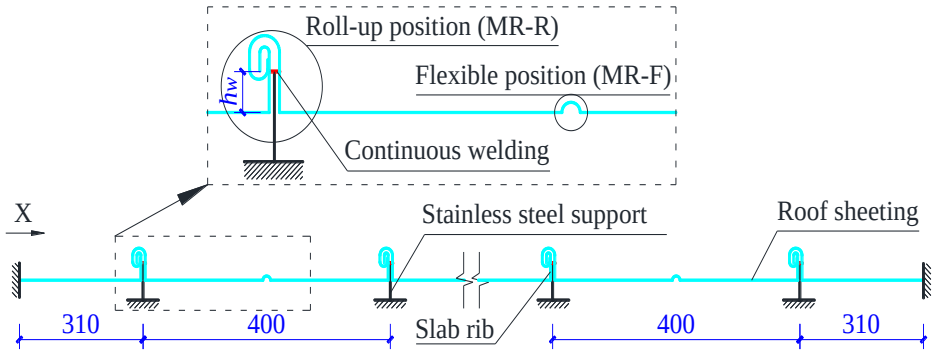

(b) Cross-section layout

Fig. 2 Layout of the computational model of the CWSSR system

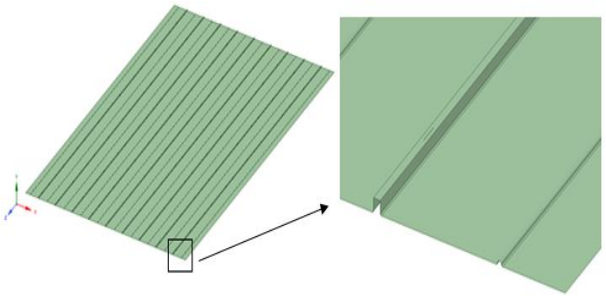

Fig. 3 Finite element model

2 Gaussian integration points in the structural members. The constitutive relationship of the metal material is defined as a bilinear elastoplastic stress-strain relationship. A strain-hardening value of 2% of the elastic stiffness, which describes the postyield stiffness and is usually 0.5%-5% of the elastic stiffness (Saatcioglu and Humar 2003), is adopted in this study. The von Mises yield criterion and associated flow rule are adopted to model the increase in the plastic strain, and both isotropic and kinematic strain hardening is considered. Fig. 3 shows the finite element model and local details. Static ultimate wind uplift loading is performed with ASTM E1592-05 (2017). The CWSSR system is first loaded to 375 Pa, which is also the dead weight of the model to achieve a force balance condition. After that, the loading sequence is performed with successive increments that do not exceed one-sixth of the design pressure of 5,400 Pa until failure is reached. Additionally, 900 Pa and 500 Pa are determined as the loading increments before and after the design pressure of 5400 Pa, respectively. At each loading increment, the pressure loading is kept constant for no less than 60 s, and the pressure loading and unloading velocities are not less than 500 Pa/s and 300 Pa/s, respectively. The minimum pressure of unloading is 375 Pa, and the maximum pressure of loading is 10,400 Pa.

4. Investigation of the welding mechanical properties and mesh refinement

4.1 Mechanical behavior of welding joints

To investigate the mechanical properties of the welding joint of the CWSSR system, 12 tension experimental specimens are tested and have been welded with four kinds of electric currents, namely, 55 A, 60 A, 65 A and 70 A.

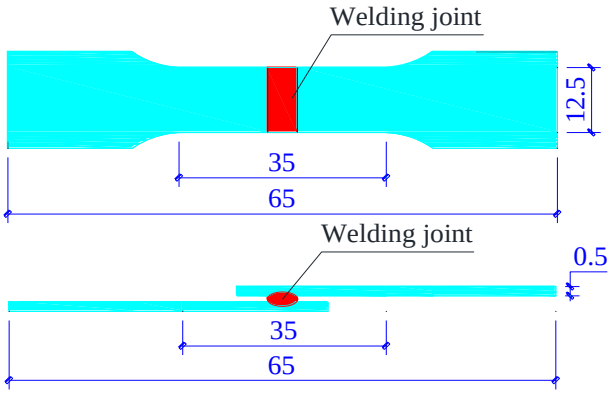

(a) Dimensions of the testing specimen

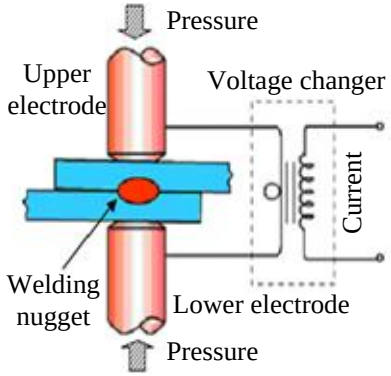

(b) Working principle of the welder

Fig. 4 Specimen dimensions and working principle of the electric-resistance welder

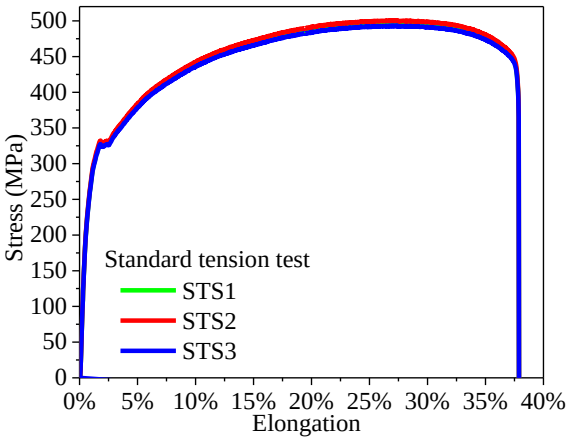

(a) Specimens STS1-STS3

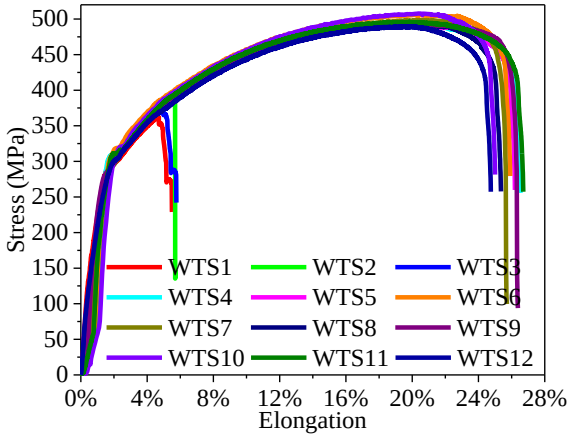

(b) Specimens WTS1-WTS12

Fig. 5 Relationship between the stress and elongation for all the specimens

Three specimens are prepared for each electric current to avoid dispersion of the testing results due to the human operation or data recording errors. These specimens are named sequentially as WTS1-WTS3 for the 55 A current, WTS4-WTS6 for the 60 A current, WTS7-WTS9 for the 65 A current, and WTS10-WTS12 for the 70 A current. All specimen dimensions are kept the same and are shown in Fig. 4(a). The welding joints are generated by an electric-resistance welder, and its working principle is shown in Fig. 4(b). Furthermore, three standard tension specimens of the base material are also prepared for comparison purposes and named STS1-STS3. In total, 15 specimens are tested. The material of all the specimens is cut from the same steel plate. The testing is carried out strictly in accordance with the code of GB/T 228.1-2010 *Metallic Materials—Tensile Testing* (*Part 1*: *Method of Test at Room Temperature*) (2010). A material testing machine with a type of DDL50 is adopted to conduct a tension experiment in a room temperature environment. The testing velocity is kept at 0.5 mm/min, and a force transducer with a capacity of 50 kN, the accuracy of ±0.5%, drift <3% per logarithmic time scale and response time of fewer than 5 μs is employed to record the testing data.

The testing results of the base material (specimens STS1-STS3) and the welding joints (specimens WTS1-WTS12) are shown in Fig. 5. The welding joints have similar mechanical behavior to that of the base material. The average values of the yield strength and ultimate strength of the base material are 329 MPa and 497 MPa, respectively. Correspondingly, the average values of the yield strength and ultimate strength are 311 MPa and 492 MPa for WTS4-WTS6, 318 MPa, and 493 MPa for WTS7-WTS9, and 300 MPa and 489 MPa for WTS10-WTS12. The strength characteristic of the welding joints is slightly smaller than that of the base material, and the welding joints of specimens WTS7-WTS9 generated by an electric current of 65 A achieve the optimal performance, which reaches 96.66% and 99.2% of yield strength and ultimate strength of the base material, respectively. Although the yield strength of specimens WTS1-WTS3 appears to be consistent with that of the other specimens, their ultimate strength is at a lower level due to early failure of the welding joints, indicating that welding joints generated by a current of 55 A are unacceptable and that a reliable connection cannot be guaranteed. Besides, the elongations of specimens WTS4-WTS12 are satisfactory and reach 26%, despite a certain degree of reduction compared with the base material. Thus, it can be concluded that the mechanical behaviors of welding joints generated with a reasonable current have excellent performance that is equivalent to that of the base material, meaning that the fixed connection adopted in the finite element model for the welding connections can be approved.

Table 1 Mesh refinement analysis of the roll-up position and the flexible position

Case		MR-R1	MR-R2	MR-R3	MR-R4	MR-F1	MR-F2	MR-F3	MR-F4
Local mesh number	Roll-up	1	2	3	4	4	4	4	4
	Flexible	9	9	9	9	1	3	6	9
Total mesh number		430388	446984	472591	498365	388516	405165	445268	498365
Local sketch of the roll-up and flexible positions		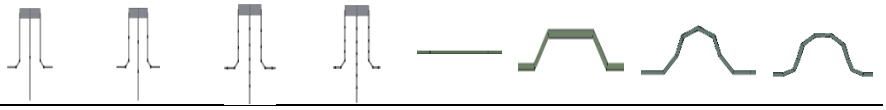							

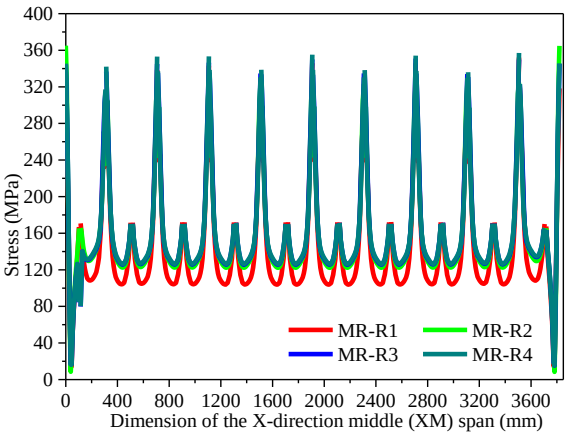

(a) Stress of the XM span

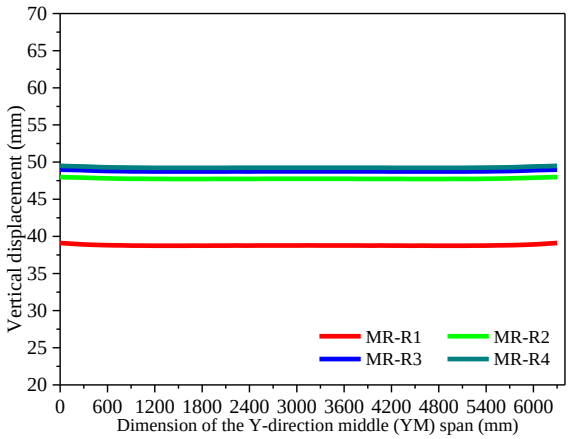

(b) Vertical displacement of the YM span

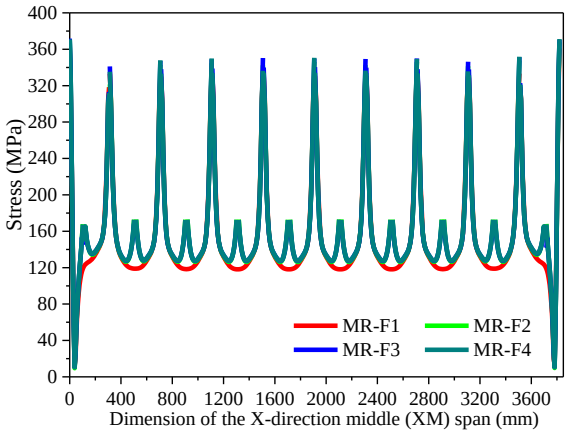

(c) Stress of the XM span

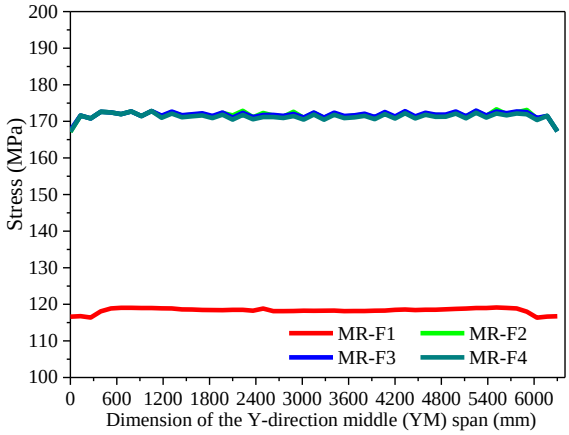

(d) Stress of the YM span

Fig. 6 Results comparison among different mesh generation methods

4.2 Mesh refinement optimization

To achieve the accurate numerical solution for the two key positions, investigations on the MR-R and MR-F positions with four methods of mesh generation are discussed to explore optimal grid meshing, and the details are summarized in Table 1. The results for the stress and vertical displacement of the model with different mesh generation methods at the two key positions are compared in Fig. 6. The specific extraction positions of the results shown in Fig. 6, namely, the X-direction middle span and the Y-direction middle span defined as the XM span and YM span, respectively, are described in detail in Fig. 2(a).

The computational results appear increasingly close with mesh encryption, indicating that more reasonable and accurate results will be guaranteed by the encrypted mesh generation method. For example, the vertical displacements of the YM span are 39.1 mm, 47.98 mm, 48.98 mm, and 49.49 mm for the mesh generation methods of MR-R1, MR-R2, MR-R3, and MR-R4, respectively, as shown in Fig. 6(b). Similarly, the stresses of the YM span are 119.04 MPa, 171.98 MPa, 172.45 MPa, and 172.71 MPa for the mesh generation methods of MR-F1, MR-F2, MR-F3, and MR-F4, respectively, as shown in Fig. 6(d). The mesh generation methods of MR-R1 and MR-F1 show the poorest performance, meaning that it is necessary and important to perform encrypted mesh generation at the two key positions of the model. For the other mesh generation methods, namely, MR-R2~R4 and MR-F2~F4, the results in Fig. 6 appear to be similar, which means that all three mesh generation methods for the two key positions are acceptable. However, it is well known that computational time will gradually increase exponentially with encrypted mesh generation (Wang and Wu 2019). Thus, considering

(a) Roof sheeting

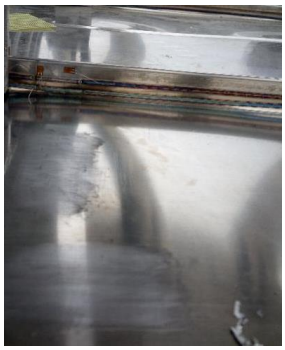

(b) Roof sheeting

(c) Roof sheeting

(c) Support of the roof sheeting

(d) Secondary batten

Fig. 7 Damage observations after testing

both the time and accuracy of the calculation, mesh encryption methods of MR-R3 and MR-F3 are finally adopted for the two key positions of the finite element model.

5. Static ultimate wind uplift testing and model validation

5.1 Testing program

The testing specimen is a full-scale specimen and has the same plane geometry and material characteristics as the finite element model adopted. To ensure that the testing investigation reflects the mechanical behaviors of real engineering, the testing specimen is manufactured based on the CWSSR system of the Zhaoqing New District Sports Center by the same fabrication factory and professional workers. All assembled members, namely, the main structure, floor layer, sound insulation layer, main and secondary battens, thermal insulation layer, leveling layer, waterproof layer, and roof sheeting layer, are included in the testing specimen. In total, 12 strain measuring points, namely, SP1-SP12, are installed at the center part of the testing specimen, as shown in Fig. 2(a). SP1 and SP2 are positioned in the longitudinal and vertical directions, respectively, and installed on the slab rib in the middle of the two supports. SP3/5 and SP4/6 are also positioned in the longitudinal and vertical directions, respectively, and are installed on the slab rib where the support is located. SP7/9/11 and SP8/10/12 are positioned in the longitudinal and transverse directions, respectively, which are all installed on the middle surface of the roof sheeting.

Static ultimate wind uplift testing of the CWSSR specimen is performed at The Twenty-Fourth Station of Quality Supervision and Inspection in Tianjin, China. The specimen is installed in a sealed chamber, which can bear a minimum uplift pressure of 20 kPa. The centrifugal fan can generate a minimum uplift of ±10 kPa on the surface of the testing specimen, which obviously meets the maximum pressure needs of 10.4 kPa, which is the maximum bearing capacity of the investigated specimen. Before testing, an air leakage measurement is performed by applying three static pressure levels of 480 Pa, 960 Pa, and 1,440 Pa ± 0.05% and maintaining each pressure for 60 ± 3 s. After that, the static ultimate wind uplift testing starts with the same loading sequence as the numerical model. Both of them meet the requirements of ASTM E1592-05 (2017). Details about the uplift wind load application can be found in the study of Ou and Wang (2020).

5.2 Testing observation

After testing, structural members of the CWSSR specimen are demolished from top to bottom to observe the damage and deformation. Fig. 7 shows the observations of the structural members. No rupture or tearing failures occurred on the roof sheeting, indicating that the roof sheeting is in the yielding stage and that the ultimate state has not yet been reached, which proves that the roof

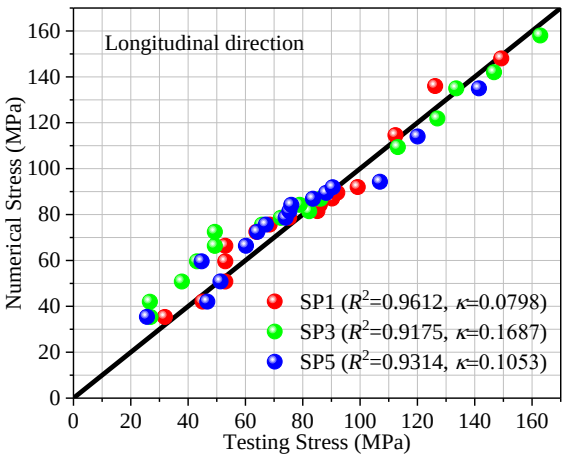

(a) Measuring points of SP1/3/5

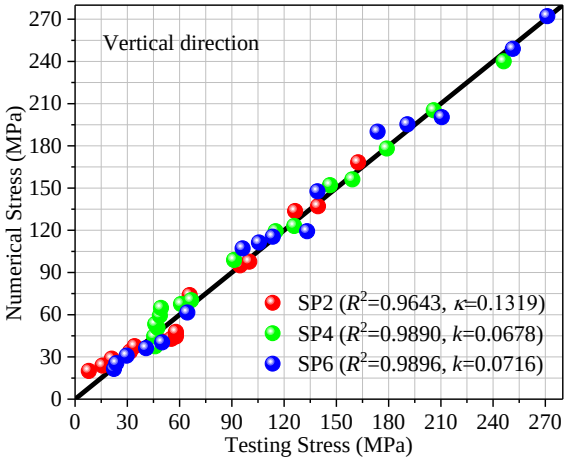

(b) Measuring points of SP2/4/6

Fig. 8 Stress comparison between the test and simulation

supports, namely, between the support and the lower

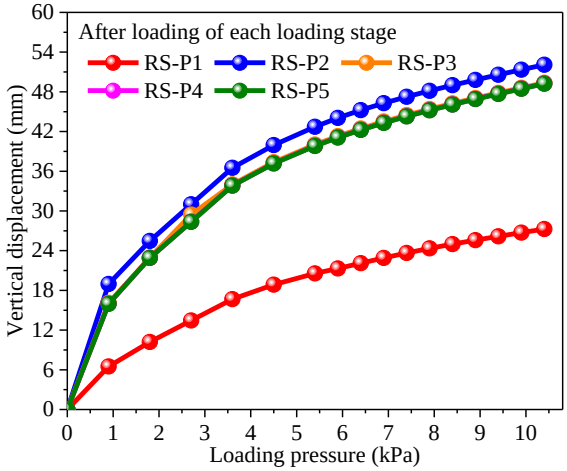

(a) After loading of each loading stage

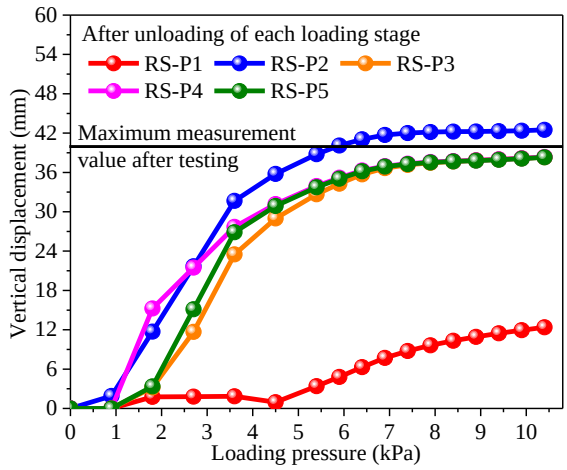

(b) After unloading of each loading stage

Fig. 9 Vertical displacement of the roof sheeting

sheeting with the CWSSR system has excellent wind resistance performance, as shown in Fig. 7(a). However, it can be found that a certain stress concentration is generated at the connection positions between the roof sheeting and its supports. This stress concentration further extends to the roof sheeting around the supports and causes a certain degree of deformation, as shown in Fig. 7(b). Besides, unrecoverable vertical deformation appears for the roof sheeting during the wind uplift loading, as shown in Fig. 7(c), which reaches a maximum value of 39.6 mm from the upper surface of the roof sheeting. However, no failure damage can be detected on the roof sheeting or the corresponding connections, indicating that the CWSSR system has a good ductile deformation capacity.

Furthermore, all welding joints between the roof sheeting, between the roof sheeting and support appear to be in perfect working condition without any failure damage, such as disengagement of the welding joints and ruptures, meaning that the continuous welding technology of the ultrapure ferritic stainless steel roof sheeting is a reliable way of ensuring an integral roof system even during strong wind excitations. In addition, the bottom connections of the secondary batten, also appear stable and undamaged. No pull-out or pull-through failures can be detected for the connections between the screw fasteners and battens, as shown in Figs. 7(c) and (d), indicating that the supports provide firm constraint to the upper roof sheeting. Thus, it can be concluded that considering only the roof sheeting and its supports and assuming a fixed connection for the lower part of the supports in the numerical model of this study are realistic ways of investigating the wind resistance performance of the CWSSR system.

The damage observations of the CWSSR system were compared with the results from other literatures studying the wind uplift capacity of different roof systems. The average ultimate capacities of all the literature cases were respectively 4.4 kPa (Standing seam roof system) (Habte and Mooneghi 2015), 7.3 kPa (Standing seam roof system) (Friedrich and Luible 2016), 4.28 kPa (Screw-fastened roof system) (Damatty and Rahman 2003), and 4.7 kPa (Screw-fastened roof system) (Henderson and Williams 2013). In addition, significant failures such as seam-clip rupture, panel-rib rupture, and seam-line disengagement were observed for both of the two kinds of typical high yield,

light gage steel standing seam metal roofs (Habte and Mooneghi 2015). Four specimens, two wood-fiber polypropylene-based wood-plastic composites (WPC) products (WPC-1; WPC-2), and two polyvinylchloride (PVC) plastics cladding products not containing fibers (PVC-1; PVC-2), were tested. Rupture failure of the cladding occurred for both the WPC and the PVC specimens (Friedrich and Luible 2016). The results indicated that the standing seam metal roof failure was governed by the seam-clip opening (Damatty and Rahman 2003). Failure mechanisms of both the oriented strand board (OSB) and the plywood roofs were pull-out and pull-over failures at their fasteners (Henderson and Williams 2013).

The comparison showed that the CWSSR system has a strong resistance deformation capacity, which is approximately two times of those of the other roof systems, and a strong bearing capacity in high winds. Only local plastic deformation with warpage and bending damage can be detected for the roof sheeting of the CWSSR system under pressures of almost 10.4 kPa. There are no tearing or rupture failures for the panels, fasteners and connections of the CWSSR system. However, significant failures can be found for other roof systems, such as clip and rib ruptures (Habte and Mooneghi 2015), panel rupture (Friedrich and Luible 2016), seam disengagement (Damatty and Rahman 2003), and fastener pull-out and pull-over failures (Henderson and Williams 2013).

5.3 Model validation

Fitting is performed between the testing and numerical analysis results with the implementation of the Levenberg-Marquardt minimization algorithm, which is widely adopted for fitting testing data (Holzapfel and Gasser 2005). The quality of the data fitting can be evaluated by the coefficient of determination R^2 and normalized mean square root error κ, which are considered to be a perfect fitting if R^2 is close to 1 and κ is close to 0 (Wang and He 2018). Comparisons of the stress data between the test and simulation are shown in Fig. 8 for the strain measuring points of SP1-SP6. All six strain measuring points are on the slab rib between the roof sheeting, and specific positions can be found in detail in Fig. 2(b). The data from the numerical simulation fit well with those of the test with acceptable fitting errors. For example, the fitting errors of (R^2, κ) are (0.9612, 0.0798) for the measuring point of SP3, (0.989, 0.0678) for SP4, and (0.9896, 0.0716) for SP6. Both the determination coefficient and normalized mean square root error of these measuring points appear to be close to the optimum values of 1 and 0, respectively, which indicates that the numerical model in this study can accurately capture the mechanical properties of the CWSSR system.

Fig. 9 shows the vertical displacement of the roof sheeting after loading and unloading of each loading stage, in which RS-P is the selection point of roof sheeting, and the corresponding specific positions of RS-P1-P5 are shown in Fig. 2(b). The vertical displacements all appear to increase with increasing loading pressures, and the measuring point of RS-P2 shows the maximum vertical deformation. Except for the side span point of RS-P1 with a smaller vertical displacement during the loading process, the other points of RS-P2-P5 have a similar vertical displacement at each loading increment. For example, as shown in Fig. 9(a), the displacements are 24.99 mm, 49 mm, 46.25 mm, 45.24 mm, and 45.2 mm for RS-P1, RS-P2, RS-P3, RS-P4, and RS-P5, respectively, after loading of the loading pressure stage of 8.4 kPa. Correspondingly, the displacements are 10.33 mm, 44.43 mm, 37.46 mm, 37.58 mm and 37.52 mm after unloading of the loading pressure stage of 8.4 kPa. In addition, the maximum vertical displacement obtained from the specimen testing is 39.6 mm, as shown in Fig. 9(b), which is basically consistent with that from the numerical simulation, namely, 42.48 mm. The error between the two maximum values is only 7.3%, which further proves the reliability of the numerical program adopted in this study.

6. Parameter effects

6.1 Computational cases

It can be confirmed that numerical analysis is an effective and feasible technology for capturing the mechanical behaviors of the CWSSR system, as verified in the previous sections. To further investigate the effect of different parameters, namely, the roof sheeting thickness, roof sheeting width, and welding joint height, on the wind resistance performance of the CWSSR system, 14 full-scale models are established based on the ANSYS platform. Table 2 shows the specific parameter values of the cases. For comparison, the total model length along the longitudinal direction and the support spacing are kept the same as in the previous testing investigation, namely, 6300 mm and 300 mm, respectively. Eight pieces of the roof sheeting along the transverse direction are designed, and continuous welding is adopted among the roof sheets, which is also the same as the previous test.

6.2 Effect if the width of the roof sheeting

The vertical displacement and stress responses of the XM span of the CWSSR system with different widths of roof sheeting are shown in Fig. 10 after the loading is complete. It can be found that there is basically a coincident tendency for both the displacement and stress responses along with the X-direction distance among the different widths. For the vertical displacement response, the maximum value appears at the center of the roof sheeting, and the minimum appears near the supports, namely, the welding positions between the roof sheeting. For the structural vertical stress, the maximum appears near the supports because of the stress concentration effect, followed by the center of the roof sheeting. Besides, the structural responses show similar changing phenomena among the eight roof sheeting members for the same computational case during wind uplift excitation, indicating that the structural internal force and deformation of the CWSSR

Table 2 Details of the parameter investigation of the CWSSR system (unit: mm)

Case	Model geometry		Roof sheeting			Welding height
	Length	Width	Width	Thickness	Length	
1-4	6300	232.5+8×300+232.5 310+8×400+310 387.5+8×500+387.5 465+8×600+465	300/400 /500/600	0.5	6300	17
5-9	6300	310+8×400+310	400	).4/0.45/0.5/0.55/0.(	6300	17
10-14	6300	310+8×400+310	400	0.5	6300	15/16/17/18/19

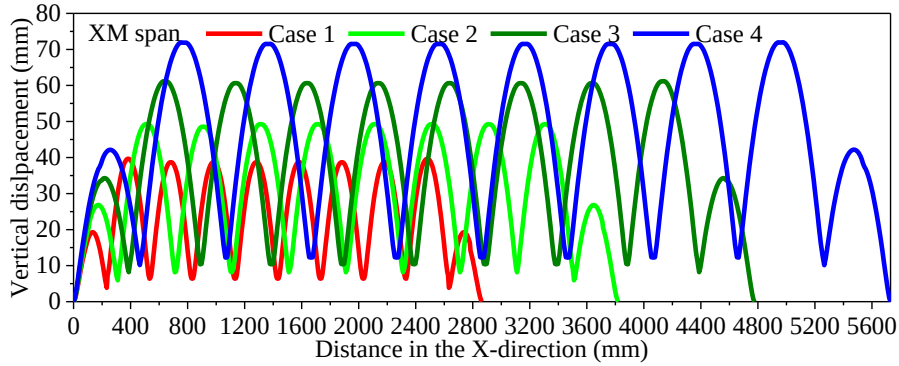

(a) Vertical displacement of the XM span

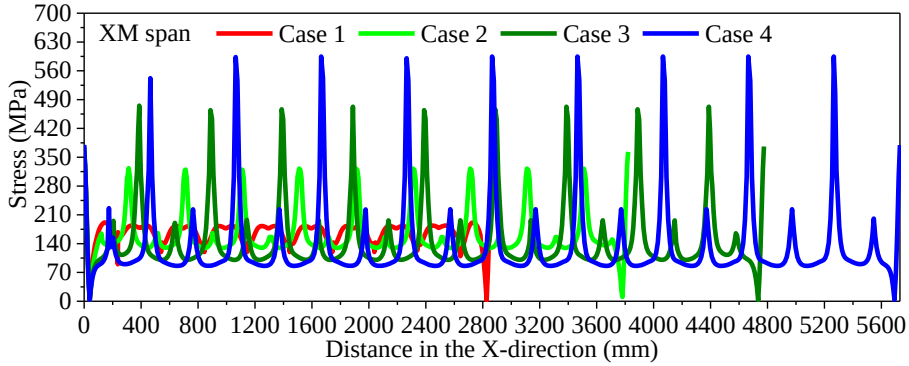

(b) Vertical stress of the XM span

Fig. 10 Displacement and stress of the CWSSR system for different widths of roof sheeting

system of each roof sheeting can be treated as independent with less interference among each other during static wind uplift loading. In other words, the wind loading is undertaken first by the roof sheeting and then transferred to the welding connection and finally to the supports on both sides. The wind-induced responses of a roof sheeting have an insignificant influence on an adjacent roof sheeting.

With increasing wind uplift loading, both the stress and displacement responses gradually increase, as shown in Fig. 11 for the two typical points at the side of the local reference support and the middle of the local reference plane, respectively. The internal force and deformation appear to linearly increase with increasing pressure for the side point (Fig. 11(a)), while they exponentially increase for the middle point (Fig. 11(b)), namely, increasing swiftly at first and then slowly increases. The structural displacement responses of the side point are less than those of the middle point, while the stress responses of the former are greater than those of the latter. For example, the displacement responses of the side and middle points for case 3 are 10.5 mm (Fig. 11(a)) and 61.1 mm (Fig. 11(b)), respectively, at a loading pressure of 10.4 kPa; correspondingly, the stress responses are 480.2 MPa (Fig. 11(c)) and 192.7 MPa (Fig. 11(d)).

With the increasing width of the roof sheeting, the structural responses are predominantly amplified for the side and middle point. For example, the vertical displacements of the side point are 6.2 mm, 8.3 mm, 10.5 mm, and 12.9 mm for case 1 to case 4, at a loading pressure of 10.4 kPa (Fig. 11(a)). Similarly, the vertical displacements of the middle point are 36.3 mm, 49.2 mm, 61.1 mm, and 73.9 mm for case 1 to case 4, at the same loading pressure (Fig. 11(b)). Obviously, the displacement response is amplified by more than two times as the width increases from 300 mm to 600 mm. Moreover, the vertical stresses of the side point are 182.8 MPa and 613.8 MPa for case 1 and case 4, respectively, namely, the latter is more than three times that of the former. Thus, it can be concluded that the width of the roof sheeting has a significant effect on the wind-resistance performance of the CWSSR system and that a larger width can greatly amplify the structural responses during wind uplift loading,

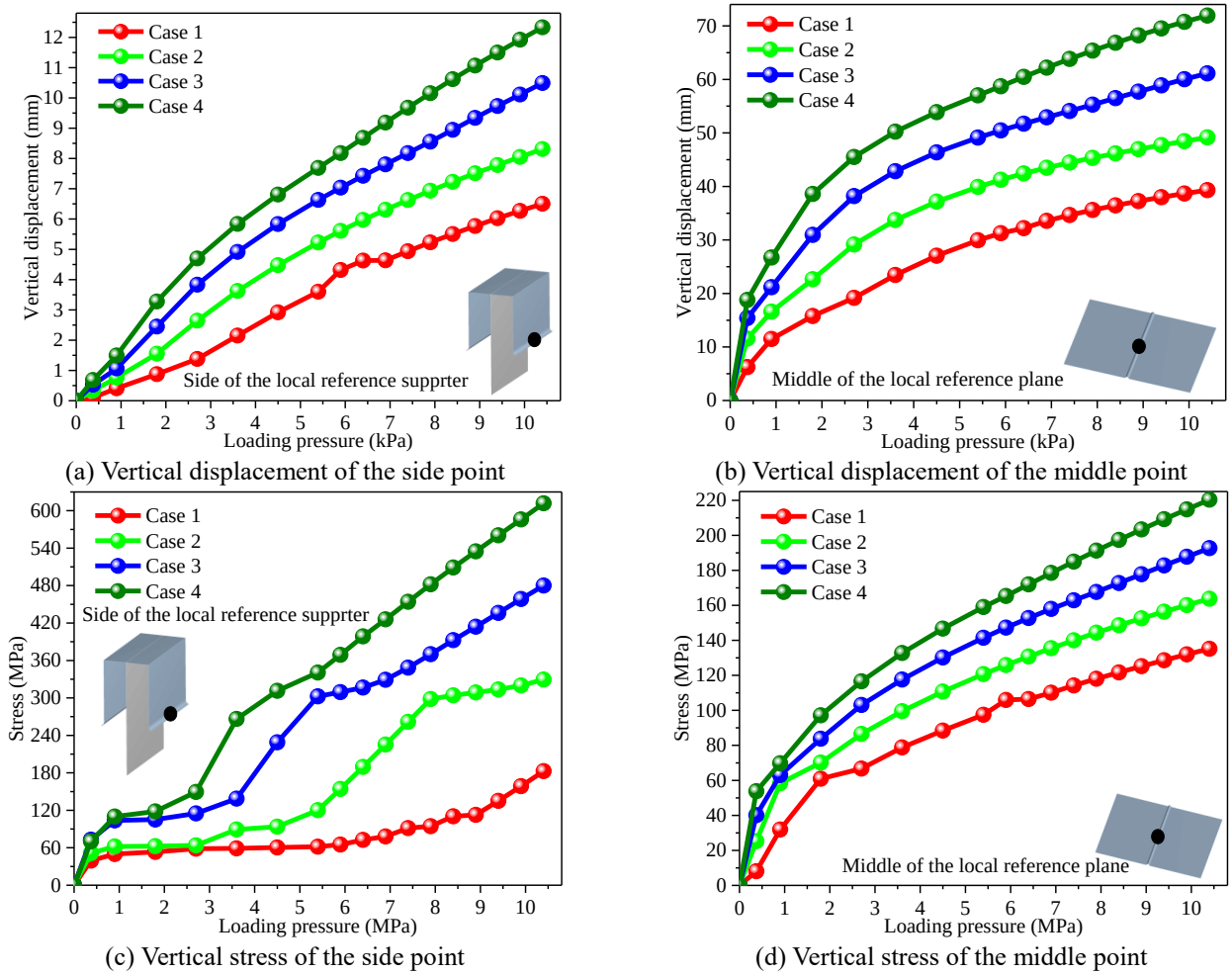

(a) Vertical displacement of the side point

(b) Vertical displacement of the middle point

(c) Vertical stress of the side point

(d) Vertical stress of the middle point

Fig. 11 Relationship between the loading pressure and structural response

especially for the structural members around the supports.

6.3 Effect of the thickness of the roof sheeting

The vertical displacement and stress responses of the CWSSR system with different roof sheeting thicknesses are shown in Fig. 12 after a final loading of 10.4 kPa. Except for the side roof sheeting of the CWSSR system, the changing tendency of the wind-induced responses is similar for the same computational cases, which proves again that the independent vibration response of the roof sheeting can be found. The maximum deformation response appears in the middle of each roof sheeting, and the corresponding minimum appears at the welding connection between the roof sheeting, as shown in Fig. 12(a). The predominant stress concentration effect also occurs at the connection supports, which is several times than that of the stress in the middle of the roof sheeting, as shown in Fig. 12(b). For example, the maximum vertical stresses are 481.5 MPa, 382.9 MPa, 318.7 MPa, 282.7 MPa and 182.6 MPa for case 5 to case 9; correspondingly, the stresses at the middle of the roof sheeting are 182.4 MPa, 166.3 MPa, 155.7 MPa, 150.4 MPa, and 147.4 MPa. It can then be concluded that a change in the thickness of the roof sheeting has much more influence on the vertical stress of the connection positions than that of the middle of the roof sheeting and the design of a reasonable thickness for the roof sheeting is necessary to avoid excessive internal force that causes structural damage to the CWSSR system.

Further investigation of the structural response with loading pressure is shown in Fig. 13 for the side and middle points of the local reference support and plane. Both displacement and stress responses appear to increase with increasing loading pressure with a linear trend for the side point and an exponential trend for the middle point, which is the same as that of the width of the roof sheeting, as discussed in the last section. The middle of the roof sheeting has a larger vertical deformation and smaller structural stress, while the side of the support has a smaller vertical deformation and larger structural stress. For example, the displacements at the side point are 12.4 mm, 10 mm, 8.3 mm, 7.1 mm and 6 mm for cases 5-9 (Fig. 13(a)), corresponding to 59.5 mm, 53.6 mm, 49.2 mm, 45.8 mm and 42.9 mm for the middle point of the five cases (Fig. 13(b)). Although the maximum deformation and stress appear at different positions of the CWSSR system, both have coincident change tendencies with the loading pressures, indicating that a reasonable thickness for the roof sheeting can achieve the optimal wind-resistance performance for avoiding excessive deformation and stress.

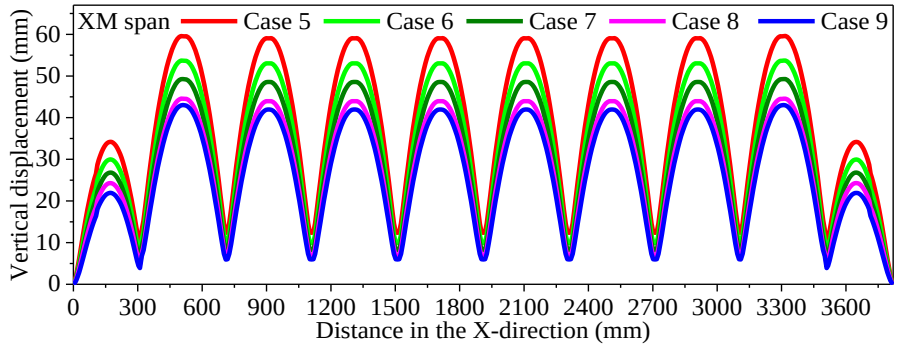

(a) Vertical displacement of the XM span

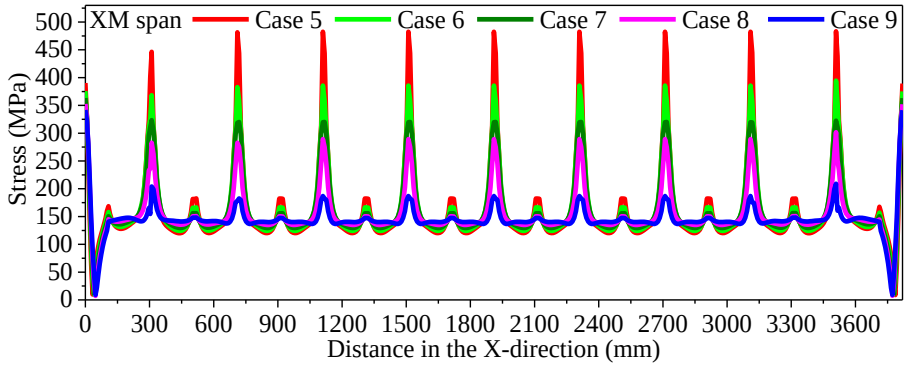

(b) Vertical stress of the XM span

Fig. 12 Displacement and stress of the CWSSR system for different roof sheet thicknesses

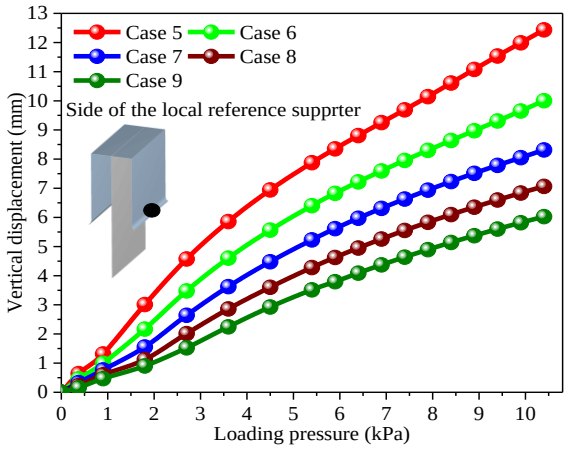

(a) Vertical displacement of the side point

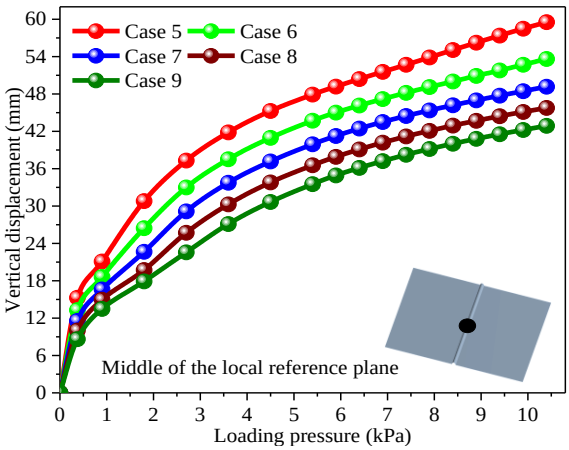

(b) Vertical displacement of the middle point

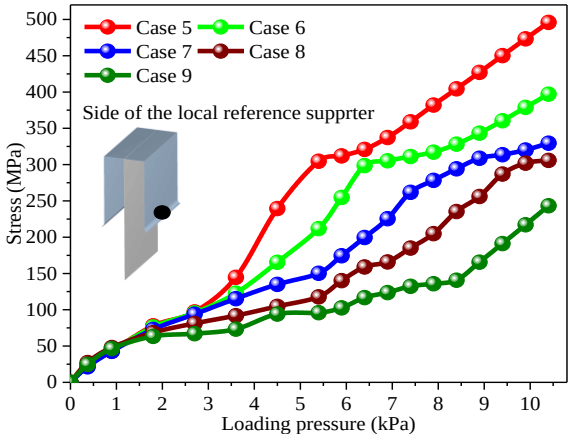

c) Vertical stress of the side point

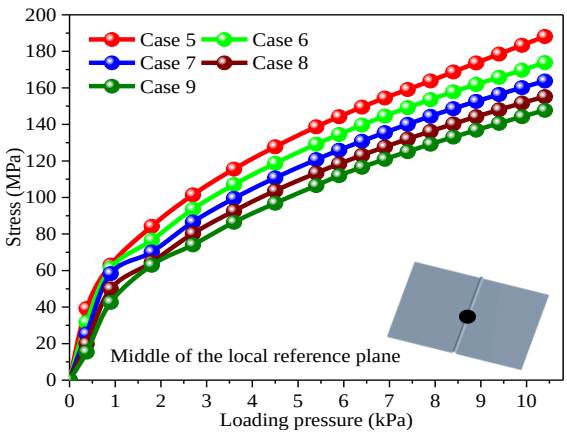

(d) Vertical stress of the middle point

Fig. 13 Relationship between the loading pressure and structural response

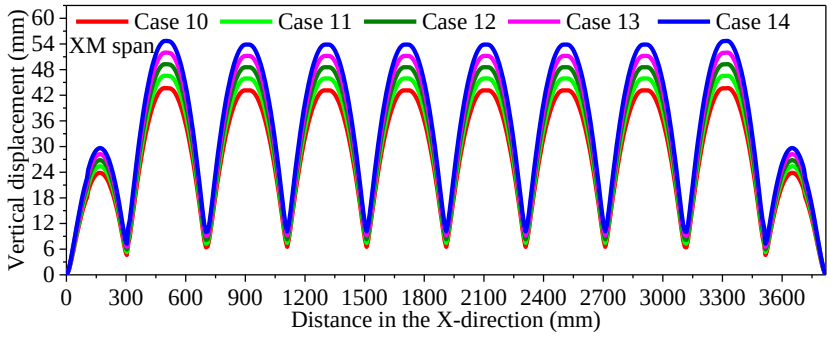

(a) Vertical displacement of the XM span

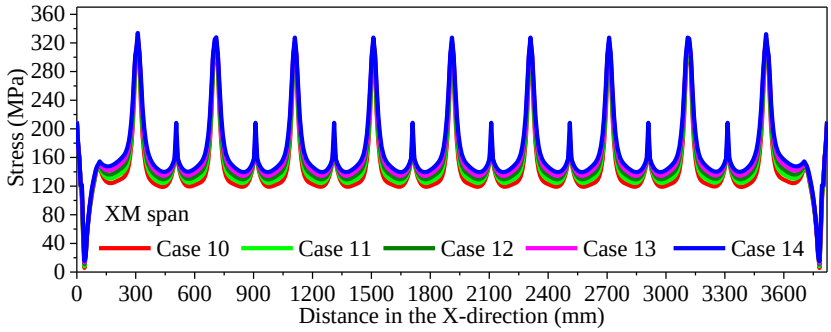

(b) Vertical stress of the XM span

Fig. 14 Displacement and stress of the CWSSR system at different welding heights

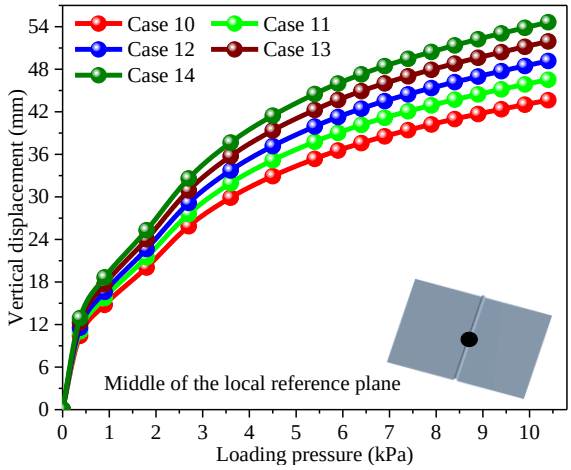

(a) Vertical stress of the middle point

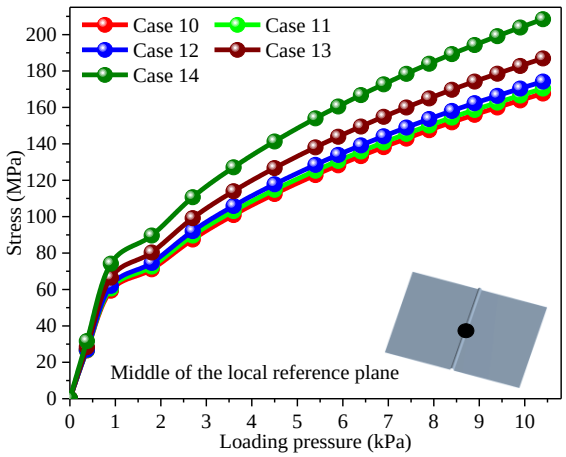

(b) Vertical stress of the middle point

Fig. 15 Relationship between the loading pressure and structural response

6.4 Effect of the welding height

Fig. 14 shows the vertical displacement and stress responses of the XM span, and Fig. 15 shows the changing tendency of the two responses with the loading pressures. The vertical deformation and stress at the middle of the roof sheeting are influenced by changing the welding height to a certain extent, which appears to increase with increasing welding height, as shown in Figs 14 and 15. However, the degree of increase appears to be less significant for both the vertical deformation and stress. For example, the vertical displacements at the middle point are 43.6 mm, 46.5 mm, 49.2 mm, 51.9 mm and 54.6 mm for cases 10-14 at a loading pressure of 10.4 kPa (Fig. 15(a)), in which the last displacement is only 1.25 times that of the first displacement. Similarly, the stresses at the same point are 167.6 MPa, 170.3 MPa, 174.2 MPa, 186.8 MPa, and 208.4 MPa for cases 10-14 (Fig. 15(b)), in which the last is only 1.24 times that of the first.

Furthermore, changing the investigated welding height, namely, from 15 mm to 19 mm, has a negligible influence on the vertical stress for the structural members around the supports, as shown in Fig. 14(b). Although there is a certain stress concentration effect at the connection positions, no amplification phenomenon of the stress concentration is aroused by changing the welding height, which is different from that of the width and thickness of the roof sheeting. For example, the maximum vertical stresses are 317.8 MPa,

320.2 MPa, 323.4 MPa, 328.7 MPa, and 333.9 MPa for cases 10-14, in which the last is only 1.05 times that of the first.

Furthermore, changing the investigated welding height, namely, from 15 mm to 19 mm, has a negligible influence on the vertical stress for the structural members around the supports, as shown in Fig. 14(b). Although there is a certain stress concentration effect at the connection positions, no amplification phenomenon of the stress concentration is aroused by changing the welding height, which is different from that of the width and thickness of the roof sheeting. For example, the maximum vertical stresses are 317.8 MPa, 320.2 MPa, 323.4 MPa, 328.7 MPa, and 333.9 MPa for cases 10-14, in which the last is only 1.05 times that of the first.

7. Conclusions

The CWSSR system is the focus of this study with full-scale testing and numerical simulation to explore the wind-resistance capacity during static ultimate uplift loading. The following conclusions can be drawn:

- As for the Type 445J2 stainless steel with the thickness of 0.5 mm, the welding joint with 65 A current achieves the best connection performance with the yield and ultimate strength reaching 96.66% and 99.2% of the base material, respectively, which also has a satisfactory elongation of 26% to ensure a favorable deformation capacity.
- Excellent ultimate wind-resistant performance of the investigated CWSSR system is confirmed by full-scale testing without any rupture or tearing failure for all roof sheeting, welding, and screw connections and roof supports. Certain stress concentrations are generated and further extend to the roof sheeting around the supports.
- The structural response of the roof sheeting can be defined to be independent of each other and has less interference with its adjacent roof sheeting. The maximum deformation and stress appear in the middle of the roof sheeting and at the connection supports, respectively, and the latter produces a serious stress concentration effect.
- Both the width and thickness of the roof sheeting have a predominant influence on the responses of the vertical deformation and internal force of the CWSSR system, which appear to increase with increasing width and decreasing thickness. The response amplification effect even produces an increase that is three times that of the original value. The welding height has an insignificant influence on the responses of the CWSSR system.

Acknowledgments

This project is supported by the National Natural Science Foundation of China (51878191, 51778162), Natural Science Foundation of Guangdong Province (2020A1515010994) and Guangzhou Yangcheng scholars project (202032866).

References

Ansys release 14.0 (2011), "ANSYS-CFX: CFX Introduction, CFX Reference Guide, CFX Tutorials, CFX-Pre User's Guide, CFX-Solver Manager User's Guide, CFX-Solver Modeling Guide, CFX-Solver Theory Guide", Ansys Inc., U.S.A.

ASTM E1592-05 (2017), *Standard test method for structural performance of sheet metal roof and siding systems by uniform static air pressure difference*, ASTM International.

ASTM E1592-05 (2017), *Standard test method for structural performance of sheet metal roof and siding systems by uniform static air pressure difference*, ASTM International.

Banks, D. and Meroney, R.N. (2001), "A model of roof-top surface pressures produced by conical vortices: model development", *Wind Struct.*, **4**(3). https://doi.org/10.12989/was.2001.4.3.227.

Baskaran, A., Molleti, S. and Roodvoets, D. (2007), "Understanding low-sloped roofs under Hurricane Charley from field to practice", *J. ASTM Int.*, **4**(10), 1-13. https://doi.org/10.1520/STP45373S.

Boughton, G.N. and Falck, D.J. (2007), "*Tropical Cyclone George Damage to Buildings in the Port Hedland Area*", Technical Report 52, Cyclone Testing Station, James Cook University, Townsville, Australia.

CSA-A123.21-14 (2015), *Standard test method for the dynamic wind uplift resistance of membrane-roofing systems,* Standards Council of Canada.

Dabral, A. and Ewing, B.T. (2009), "Analysis of wind-induced economic losses resulting from roof damage to a metal building", *J. Business Valuation Economic Loss Analy.*, **4**(2), 10-20. https://doi.org/10.2202/1932-9156.1054.

El Damatty, A.A., Rahman, M. and Ragheb, O. (2003), "Component testing and finite modeling of standing seam roofs", *Thin-Walled Struct.*, **41**, 1053-1072. https://doi.org/10.1016/S0263-8231(03)00048-X.

Friedrich, D. and Luible, A. (2016), "Measuring the wind uplift capacity of plastics-based cladding using foil bag tests: A comparative study", *J. Build. Eng.*, **8**, 152-161. https://doi.org/10.1016/j.jobe.2016.10.009.

GB/T 228.1-2010 (2010), "*Metallic Materials-Tensile Testing* (*Part 1*: *Method of Test at Room Temperature*)", Standardization Administration of the People's Republic of China, Beijing.

Habte, F., Mooneghi, M.A., Chowdhury A.G. and Irwin, P. (2015), "Full-scale testing to evaluate the performance of standing seam metal roofs under simulated wind loading", *Eng. Struct.*, **105**, 231-248. https://doi.org/10.1016/j.engstruct.2015.10.006.

Henderson, D., Williams, C., Gavanski, E. and Kopp, G.A. (2013), "Failure mechanisms of roof sheathing under fluctuating wind loads", *J. Wind Eng. Ind. Aerod.*, **114**, 27-37. https://doi.org/10.1016/j.jweia.2013.01.002.

Holmes, J.D. (2015), *Wind loading of structures*, CRC Press, Oakville, Canada.

Holzapfel, G.A., Gasser, C.T., Sommer, G. and Regitnig, P. (2005), "Determination of the layer-specific mechanical properties of human coronary arteries with non-atherosclerotic intimal thickening, and related constitutive modelling", *Amer. J. Physiol. Heart Circulatory Physiol.*, **289**, H2048-H2058. https://doi.org/10.1152/ajpheart.00934.2004.

Huang, G., He, H., Mehta, K.C. and Liu, X. (2015), "Data-based probabilistic damage estimation for asphalt shingle roofing", *J. Struct. Eng.*, **141**(12), 04015065. https://doi.org/10.1061/(ASCE)ST.1943-541X.0001300.

Ji, X.W., Huang, G.Q., Zhang, X.X. and Kopp, G.A. (2018), "Vulnerability analysis of steel roofing cladding: Influence of wind directionality", *Eng, Struct.,* **156**, 587-597. https://doi.org/10.1016/j.engstruct.2017.11.068.

Ji, X.W., Huang, G.Q., Zhang, X.X. and Kopp, G.A. (2018),

"Vulnerability analysis of steel roofing cladding: influence of wind directionality", *Eng. Struct.*, **156**, 587-597. https://doi.org/10.1016/j.engstruct.2017.11.068.

Konthesingha, K.M.C., Stewart, M.G., Ryan, P. and Ginger, J., Henderson, D. (2015), "Reliability based vulnerability modelling of metal-clad industrial buildings to extreme wind loading for cyclonic regions", *J. Wind Eng. Ind. Aerod.*, **147**, 176-185. https://doi.org/10.1016/j.jweia.2015.10.002.

Li, Y. and Ellingwood, B.R. (2006), "Hurricane damage to residential construction in the us: Importance of uncertainty modeling in risk assessment", *Eng. Struct.*, **28**(7), 1009-1018. https://doi.org/10.1016/j.engstruct.2005.11.005.

Lovisa, A.C., Wang, V.Z., Henderson, D.J. and Ginger, J.D. (2013), "Development and validation of a numerical model for steel roof cladding subject to static uplift loads", *Wind Struct.*, **17**(5), 495-513. https://doi.org/10.12989/was.2013.17.5.495.

Luo, N., Liao, H. and Li, M. (2017), "An efficient method for universal equivalent static wind loads on long-span roof structures", *Wind Struct.*, **25**(5), 493-506. https://doi.org/10.12989/was.2017.25.5.493.

Mahaarachchi, D. and Mahendran, M. (2009), "Wind uplift strength of trapezoidal steel cladding with closely spaced ribs", *J. Wind Eng. Ind. Aerod.*, **97**, 140-150. https://doi.org/10.1016/j.jweia.2009.03.002.

Mahendran, M. (1995), "Wind-resistant low-rise buildings in the tropics", *J. Perform. Construct. Facilities*, **9**(4), 330-346. https://doi.org/10.1061/(ASCE)0887-3828(1995)9:4(330).

Mahendran, M. (1997), "Review of current test methods for screwed connections", *J. Struct. Eng.*, **123**, 321-325. https://doi.org/10.1061/(ASCE)0733-9445(1997)123:3(321).

Mahendran, M. and Tang, R.B. (1998), "Pull-out strength of steel roof and wall cladding systems", *J. Struct. Eng.*, **124**(10), 1192-1201. https://doi.org/10.1061/(ASCE)0733-9445(1998)124:10(1192).

NIST (2006), "*Performance of physical structures in Hurricane Katrina and Hurricane Rita: a reconnaissance report*", Gaithersburg, MD, National Institute of Standards and Technology.

Ou, T., Wang, D.Y., Xin, Z.Y., Tan, J., Wu, C.Q., Guo, Q.W. and Zhang, Y.S. (2020), "Full-scale tests on the mechanical behaviour of a continuously welded stainless steel roof under wind excitation", *Thin-Walled Struct.*, **150**, 106680. https://doi.org/10.1016/j.tws.2020.106680.

Saatcioglu, M. and Humar, J. (2003), "Dynamic analysis of buildings for earthquake resistant design", *Canadian J. Civil Eng.*, **30**, 338-359. https://doi.org/10.1139/l02-108.

Sivapathasundaram, M. and Mahendran, M. (2016), "Experimental studies of thin-walled steel roof battens subject to pull-through failures", *Eng. Struct.* **113**, 388-406. https://doi.org/10.1016/j.engstruct.2015.12.016.

Sivapathasundaram, M. and Mahendran, M. (2018), "New pull-through capacity equations for the design of screw fastener connections in steel cladding systems", *Thin-Walled Struct.*, **122**, 439-451. https://doi.org/10.1016/j.tws.2017.08.019.

Stathopoulos, T., Wang, K. and Wu, H. (2001), "Wind pressure provisions for gable roofs of intermediate roof slope", *Wind Struct.*, **4**(2), 119-130. https://doi.org/10.12989/WAS.2001.4.2.119.

Uematsu, Y. and Yamada, M. (2002), "Wind-induced dynamic response and its load estimation for structural frames of circular flat roofs with long spans", *Wind Struct.*, **5**(1), 49-60. https://doi.org/10.12989/was.2002.5.1.049.

Wang, D.Y., He, C.B., Wu, C.Q. and Zhang, Y.S. (2018), "Mechanical behaviors of tension and relaxation of tongue and soft palate: Experimental and analytical modeling", *J. Theoretic. Biology*, **459**, 142-153. https://doi.org/10.1016/j.jtbi.2018.10.001.

Wang, D.Y., Tse, K.T., Zhou, Y. and Li, Q.X. (2015), "Structural performance and cost analysis of wind-induced vibration control schemes for a real super-tall building", *Struct. Infrastruct. Eng.*, **11**(8), 990-1011. https://doi.org/10.1080/15732479.2014.925941.

Wang, D.Y., Wu, C.Q., Zhang, Y.S., Ding, Z.X. and Chen, W.R. (2019). "Elastic-plastic behavior of AP1000 nuclear island structure under mainshock-aftershock sequences", *Annals Nuclear Energy*, **123**, 1-17. https://doi.org/10.1016/j.anucene.2018.09.015.

Wang, D.Y., Zhuang, C.L. and Zhang, Y.S. (2018), "Seismic responses characteristics of base-isolated AP1000 nuclear shield building subjected to beyond-design basis earthquake shaking", *Nuclear Eng. Technol.*, **50**(1), 170-181. https://doi.org/10.1016/j.net.2017.10.005.

Xu, Y.L. and Reardon, G.F. (1993), "Test of screw fastened profiled roofing sheets subject to simulated wind uplift", *Eng. Struct.*, **15**(6), 423-430. https://doi.org/10.1016/0141-0296(93)90060-H.

Zhao, M. and Gu, M. (2011), "Database-assisted wind vulnerability assessment for metal buildings", *Proceeding of 13th International Conference on Wind Engineering*, Amsterdam, Netherlands.

AD